Express Polymer Letters Vol.18, No.10 (2024) 1008–1022
Available online at www.expresspolymlett.com
https://doi.org/10.3144/expresspolymlett.2024.77

Research article

Static and dynamic behaviour of ultra high molecular weight poly-ethylene (UHMWPE) Tensylon® composite

*Magali Castres, Aboulghit El Malki Alaoui, Camille Caisso, Martin Monloubou, Michel Arrigoni**

ENSTA Bretagne, IRDL UMR CNRS 6027 F-29806, Brest Cedex 9, France

Received 12 December 2023; accepted in revised form 9 July 2024

Abstract. Nowadays, ultra high molecular weight polyethylene (UHMWPE), allows the combination of lightweight, high strength and is praised for the design of severely loaded structures. It has become a good option for lightweight armour solutions. It is therefore important to characterise its mechanical behaviour. Up to now, strain rate effects on mechanical behaviour have been poorly explored. In this work, this issue is tackled by studying the strain rate influence on the in-plane deformation, in shear and tension of the Tensylon® HSBD30A, a UHMWPE dedicated to ballistic and blast protection. Two laminates of Tensylon® of respective orientation $[0\ °/90°]_{20}$ and $[\pm45°]_{20}$ were subjected to static and split Hopkinson tensile bar (SHTB) tests. A new mounting system was designed, and new specimen shapes were used to match the experimental setup configurations. Digital image correlation (DIC) was used to measure the in-plane strain. A significant strain-rate dependence on the material behaviour.is evidenced. Besides, results exhibit a higher strength for the $[0°/90°]_{20}$ specimen than for the $[\pm45°]_{20}$ one. Despite some limitations, the proposed setup and measurement methods allowed visualisation of strain rate effects on the stress-strain relationship for strain rates ranging from the quasi-static regime to the dynamic one (1500 s^{-1}).

Keywords: *digital image correlation, light weight armor, mechanical behaviour, Tensylon®, UHMWPE*

1. Introduction

To design and optimise lightweight armour, a predictive model based on the material characterisation is necessary. Usually, the damage scenarios for a composite under high-velocity impact are complex and show several damage and failure mechanisms such as interlaminar delamination, permanent non-linear deformation and fibre breaking within perforated layers [5–7]. Furthermore, the back-face deformation of the ballistic panel is also likely to provoke blunt trauma effects [8]. Models used to describe the dynamic behaviour of a panel during such an event can be either semi-analytical or numerical models. Cunniff's model is one of the most widespread analytical models [4]. It, however, rests upon several restrictive assumptions: fibres are uniformly loaded, and the failure response is linear from the ultimate strength to rupture of the fibre with no plasticity assumptions, associated with the low compressive strength and unloading before complete failure. In both approaches, the non-linear shear response is not considered. Recently [9] also proposed an analytical model based on Bernouilli's principle.

Performing numerical simulations allows us to refine the level of physical details. Thus, when considering the micro-mechanical properties of the orthotropic material behaviour, the linear elastic properties, the orthotropic yield surface with a non-linear hardening description, a nonlinear shock equation of state, and a three-dimensional failure criterion supplemented by a linear orthotropic softening description should be considered [10]. It is important to provide the

*Corresponding author, e-mail: michel.arrigoni@ensta-bretagne.fr

most complete description of the phenomenon that occurs during ballistic impact in order to predict accurately the mechanical behaviour of the material as performed in [11–13]. Therefore, to design lightweight armour, it is necessary to predict the mechanical behaviour and the damage of the involved material. Modelling the mechanical behaviour of composite materials requires the characterisation of linear elastic properties, damage behaviour, failure criterion, and the influence of temperature and strain rate effects.

Recently, ultra high molecular weight poly-ethylene (UHMWPE) based composite materials have been widely used, especially for ballistic protection. UHMWPE is a thermoplastic polymer made of long poly-ethylene molecular chains. They can be obtained by the gel spinning method and have a long-length chain that results in an important strength. This process permits to have a crystalline molecular structure oriented in the gel spinning direction. Afterwards, these UHMWPE fibres are coated with resin in order to form a ply. To finish, different plies are assembled and pressed with a typical cure to obtain a laminate. This process is widely described in the works of Russell *et al*. [14].

The UHMWPE-based composites are widely used for ballistic protection because they make it possible to conciliate both lightness and strength. Moreover, these kinds of materials are more affordable than aramid-based composites such as Kevlar® or other composite materials. In general, composite materials are associated with ceramic material in order to increase the efficiency of ballistic protection. It has even been associated with a ceramic coating by additive method [15], increasing interest in using UHMWPE in ballistic protection.

The experimental behaviour of various commercial UHMWPE under quasi-static regime ($\dot{\varepsilon} = 10^{-4}$; 10^{-3} s^{-1}) was already investigated in [10, 14, 17–20]. In particular, significant influences of the strain rate [14] and of the temperature [17] were reported. Moreover, it was shown that the mechanical behaviour had two different regimes: a linear one followed by a nonlinear one. Finally, various authors reported experimental issues regarding the specimen bindings [14, 18, 19]. Other studies focused on the mechanical response of UHMWPE under impact at high strain rates $\dot{\varepsilon} = [10^4; 10^5]$ s^{-1} [5, 10, 22, 23, 26, 27]. Results pointed out that UHMWPE is a perfect candidate for ballistic protection, and, therefore, its dynamic behaviour must be well characterised. To the authors' knowledge, the intermediate strain rate range ($\dot{\varepsilon}$ – few hundreds to thousand s^{-1}) has never been explored on such composite materials. There is only one study relating to the mechanical behaviour of UHMWPE yarns for intermediate strain rates [28]. These intermediate strain rates are encountered in ballistic impacts at lower velocities (≈300 to 400 m/s) and during blast loading.

The present study, therefore, aims to fill that gap in the in-plane mechanical characterisation, in shear and tension, of UHMWPE under static and dynamic loading. It could bring new insight into the determination of the constitutive behaviour of laminated rate-dependent polymers such as piezoresistive materials, as previously done in [28, 29]. More recently, some authors [30] pointed out the fact the in-plane mechanical behaviour of Dyneema® UHMWPE is very sensitive to strain rate. In addition, its Young modulus is increased by 60%, and its failure stress is increased by 40% when subjected to dynamic loading. The UHMWPE variant chosen for the present work is the Tensylon® $[0°/90°]_{20}$ HSBD30A composite made by Dupont®, Wilmington, USA. It is composed of ultra high molecular weight polyethylen (UHMWPE) fibres coated with a thermoplastic matrix [39]. The Tensylon® was manufactured by Dupont® with a typical cure in pressed plate form of 500×500 mm. Each ply has a thickness of 60 μm, thus total thickness of the studied material is 2.40 mm. This study aims to perform an experimental characterisation of the mechanical behaviour of Tensylon® under different loading rates. To this purpose, it is proposed to perform experimental campaigns for static tests using two different kinds of solicitations for uniaxial tensile tests: a monotonous and a loading/unloading. For dynamic tests, a split Hopkinson tensile bars set was used to explore the aforementioned intermediate strain rate range between 900 and 1500 s^{-1} since these strain rates are encountered by structure panels during blast and ballistic loading. Since this sample is subjected to sliding and delamination in the grips, two solutions for the sample fixation are discussed. For each solicitation, three displacement velocities were tested. Then results are presented and discussed for two laminate configurations, $[\pm45°]_{20}$ and $[0°/90°]_{20}$.

2. Quasi-static mechanical behaviour of UHMWPE

2.1. Experimental setup

Two different specimen shapes were considered: one for $[0°/90°]_{20}$ laminates and another for $[\pm45°]_{20}$ laminates. The photographs of the two different specimen shapes are available in Figure 1. The effective cross-sectional area for $[0°/90°]_{20}$ specimens are 4×2.40 mm and 18×2.40 mm for $[\pm45°]_{20}$. The effective length is 50 mm.

The experimental protocol follows EN-ISO 527 [47] standard recommendations, except for the shape of the specimens. All the tests were performed with an INSTRON 5969 electromechanical jack equipped with a 50 kN load cell with a measuring accuracy of 0.5% of the value. Three traverse speeds were considered: 0.1, 1 and 10 mm/min. For each traverse speed, at least three tests were performed for the assessment of the reproducibility. Before the specimen was clamped into the grips, black paint was sputtered, offering a speckle of a large number of small spots smaller than 1 mm. This pattern made possible the measurement of the evolution of longitudinal and transversal strains during tests by Digital Image Correlation (DIC) with a GOM 4M® system. For this study, 2D mode was used. Consequently, only the left camera was active. The lighting system was also integrated into the GOM 4M® system. The photography of the sample fixed in the tensile machine is shown in Figure 2. GOM 4M® has an acquisition frequency of 60 Hz for a strain measuring accuracy of 0.01% for a measurement range of 0.02 to 100%. The system resolution is 2448×2050 pixels for a

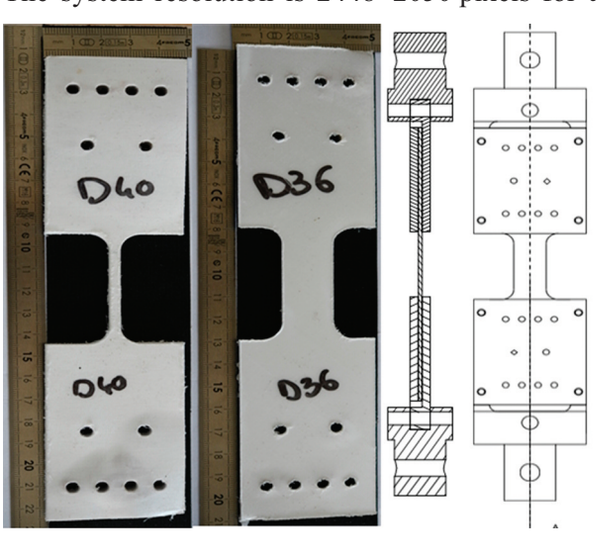

Figure 1. $[0°/90°]_{20}$ specimen on the left side, of $[\pm45°]_{20}$ laminate on the centre and a schematic of the assembly on the right side.

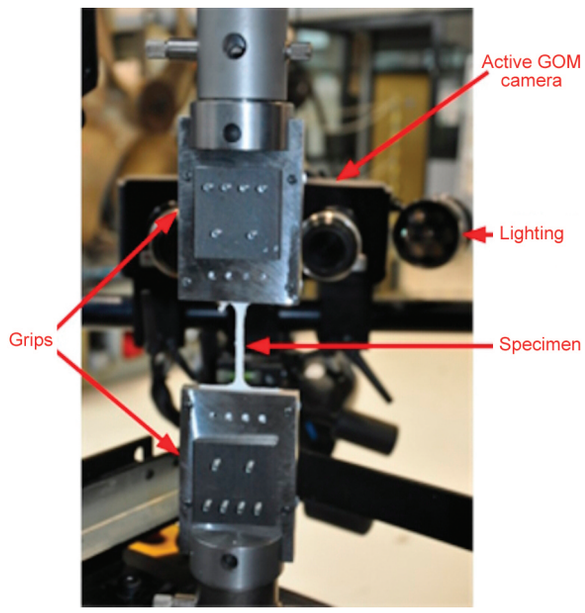

Figure 2. Assembly used to perform uniaxial tensile tests.

50 mm focal length lens. The post-treatment was performed with ARAMIS® software. For each configuration, the strain homogeneity in the considered zone was studied. For this purpose, results obtained by DIC system were considered. In Figure 3, the longitudinal strain was observed for a monotonous uniaxial tensile test at 1 mm/min for $[0°/90°]_{20}$ laminate on the left side and for $[\pm45°]_{20}$ laminate on the right side. The first picture was taken at 99 s, and the second picture at 226 s after the start of the test.

Considering results obtained for $[0°/90°]_{20}$ laminate at t = 99 s, longitudinal strain was homogeneous over the whole zone of interest. In order to obtain the stress/strain curves, an average strain was evaluated on a zone of 2×6 mm taken at the center of the zone of interest.

As previously said, DIC results obtained for $[\pm45°]_{20}$ laminate were plotted in Figure 3 on the right side. It points out three distinct zones that can be distinguished. A first zone is located near to the clamps for which longitudinal strain were around 1%. A second intermediate zone takes place below the first one and has a bow-tie shape, for which longitudinal strain was around 6%. A third one is at the centre of the specimen with a quasi-homogeneous strain of around 11%. Similar observations were reported by Berthe *et al.* [48] during the study of a [±45°] carbon/epoxy laminate. An average strain was evaluated on a zone of 2×6 mm taken at the centre of the zone of interest.

In the literature, some authors [14, 49] showed that the mechanical behaviour of UHMWPE $[0°/90°]$

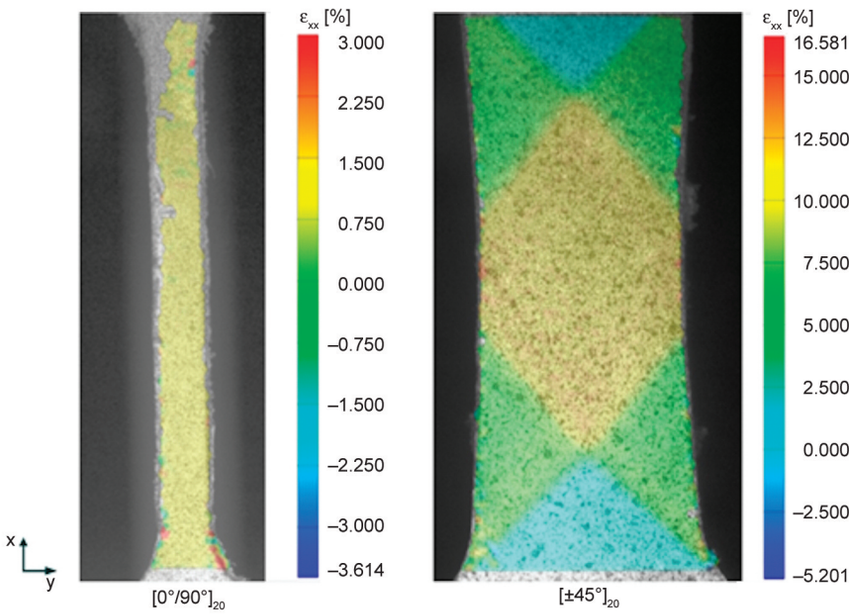

Figure 3. Digital image correlation (DIC) obtained for monotonous uniaxial tensile tests for $[0°/90°]_{20}$ at t = 99 s and 1 mm/min on the left side and for $[\pm45°]_{20}$ at t = 226 s and 1 mm/min.

laminate was visco-elasto-plastic. Therefore, it is necessary to both study elastic and plastic properties and the influence of strain rate on them. To do that, two different loading regimes can be set. All tests were uniaxial tensile tests. However, during the first campaign monotonous loads until failure were performed for three different traverse speeds and two different laminates. During the second campaign, loading/unloading tests were performed with an incremental effort of 400 N for [0°/90°] laminate and 200 N for [±45°] laminate until failure for three different traverse speeds.

2.2. Influence of strain rate on the mechanical behaviour of Tensylon® $[0°/90°]_{20}$ laminate

For uniaxial monotonous tensile tests, three traverse speeds were performed: 0.1, 1 and 10 mm/min. The corresponding strain rates were respectively: $2 \cdot 10^{-5}$, $1.5 \cdot 10^{-4}$ and $1.5 \cdot 10^{-3}$ s^{-1}. In Figure 4, stress/strain curves of the five tests performed at 10 mm/min are plotted. One may notice that the dispersion is very low. Afterwards, the stress-strain curves presented correspond to the average of five tests for a given displacement speed.

In Figure 5, the longitudinal stress–strain curves are plotted for three different strain rates. It can be seen that the mechanical behaviour of Tensylon® $[0°/90°]_{20}$ can be decomposed into two parts: a first linear behaviour followed by a second non-linear behaviour. Moreover, the mechanical behaviour

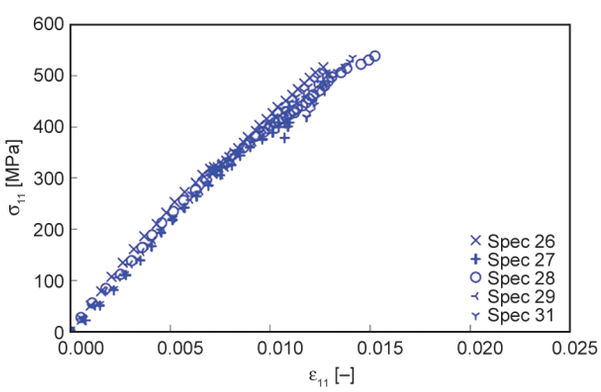

Figure 4. Tensylon® $[0°/90°]_{20}$ stress-strain curves for uniaxial monotonous tensile tests for a displacement speed of 10 mm/min and at room temperature.

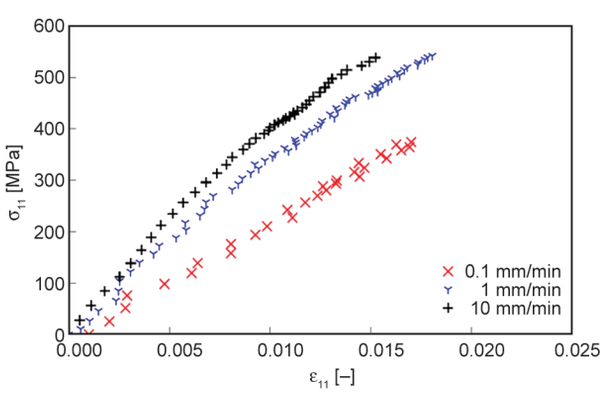

Figure 5. Tensylon® $[0°/90°]_{20}$ stress-strain curves for uniaxial monotonous tensile tests at three different strain rates and at room temperature.

seems to be strain rate dependent. These observations are in agreement with the literature [14, 49]. Indeed, considering a longitudinal strain of 0.015,

the corresponding stress is 310 MPa for 0.1 mm/min and 520 MPa for tests performed at 10 mm/min, either an increase of 68%.

In order to describe the elastic behaviour of Tensylon and its sensitivity to strain rate, Young modulus and Yield stress were evaluated for each test at each strain rate. These two values were evaluated with the method described in [50, 51]. The strain rate seems to have an important influence on the evolution of the Young modulus. When the strain rate increased from $2 \cdot 10^{-5}$ to $1.5 \cdot 10^{-3}$ s^{-1} the value of the Young modulus increased from 19.5 GPa ±7% to 45.0 GPa ±2%, that is to say an increase of 131%. Considering the evolution of the yield stress, a same trend can be observed. When the strain rate increased from $2 \cdot 10^{-5}$ to $1.5 \cdot 10^{-3}$ s^{-1} the yield stress increased from 213 MPa ±16% to 318 MPa ±2%, that is to say an increase of 49%.

In order to evaluate the influence of strain rate on the non-linear behaviour of Tensylon® $[0°/90°]_{20}$, the second experimental campaign was considered, *i.e.*, the uniaxial load/unload tensile tests. In a second step, stress-strain curve obtained during monotonous uniaxial tensile test is compared to stress-strain results obtained during loading/unloading tensile test performed at 1 mm/min. This comparison is plotted in Figure 6. The results of monotonous tensile test are represented by blue cross (+) and are slightly above that of the loading/unloading tensile test in blue solid line, even though they exhibit the same trend. The shape of the monotonous tensile test permits the description of the unloading/loading results. A first qualitative study of the influence of strain rate can be done in Figure 7 where stress-strain curves of tests performed at 0.1 and 10 mm/min are compared.

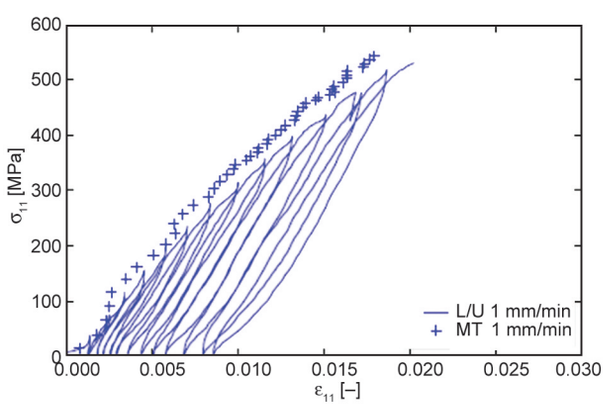

Figure 6. Comparison between stress– strain curves of the monotonous uniaxial tensile test and the loading/unloading uniaxial test performed at 1 mm/min on the Tensylon $[0°/90°]_{20}$.

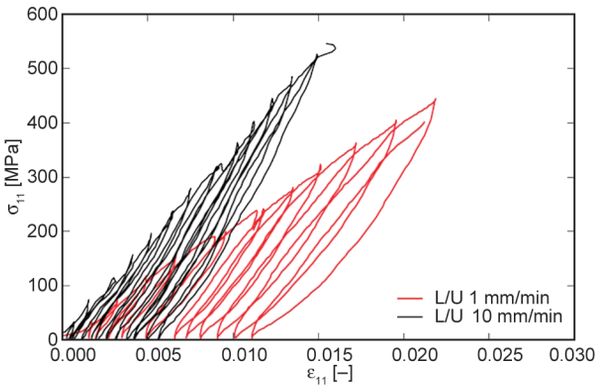

Figure 7. Tensylon® $[0°/90°]_{20}$ stress - strain curves for uniaxial loading/unloading tests at two different strain rates and at room temperature.

Strain rate appears to have an important influence on the mechanical behaviour of Tensylon® $[0°/90°]_{20}$. Indeed, at a given strain the maximum stress measured increased with the increasing strain rate. For example, for a strain of 0.015 the maximum stress measured at 10 mm/min is nearly 62% higher than the one measured at 0.1 mm/min. Moreover, strain rate seems also to influence the plastic strain and the apparent modulus for a given cycle.

2.3. Influence of strain rate on the mechanical behaviour of Tensylon® $[\pm45°]_{20}$ laminate

The mechanical shear behaviour of different UHMWPE composite was studied in the literature by various authors [14, 18, 52, 53]. In these studies, uniaxial monotonous and loading/unloading tensile tests on [±45°] laminates were performed. The authors shown that the mechanical shear behaviour was strongly and entirely non linear and was dominated by the matrix one [44, 53, 54]. However, all these studies were performed on Dyneema® UHMWPE. The matrix of the Dyneema® is a polyurethane film in contrast to Tensylon® which has a polyethylen matrix, thus different mechanical behaviours are expected and a complete study must be performed. Therefore, Tensylon® $[\pm45°]_{20}$ was subjected to tensile tests described in Section 2.2. Firstly, the influence of strain rate on the elastic properties was studied.

For uniaxial monotonous tensile tests, three traverse speeds were exerted: 0.1, 1 and 10 mm/min. The corresponding strain rates were respectively $2.2 \cdot 10^{-5}$, $1.3 \cdot 10^{-4}$ and $1.5 \cdot 10^{-3}$ s^{-1}. Five tests were performed for each configuration. In Figure 8, shear stress–shear strain curves of the five tests performed at 10 mm/min are plotted. One may notice that the dispersion is very low. The shear stress–shear strain

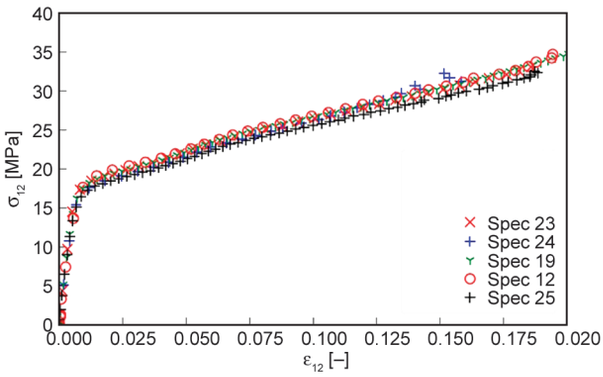

Figure 8. Tensylon® $[\pm 45°]_{20}$ shear stress–shear strain curves for uni-axial monotonous tensile tests for a displacement velocity of 10 mm/min and at room temperature.

curves presented in Figure 9–11 correspond to the average of the five tests for each strain rate.

In Figure 9, the shear stress–shear strain curves are plotted for three different strain rates. Contrary to the results obtained by Iannucci *et al*. [53], the mechanical shear behaviour of Tensylon® can be decomposed into two parts: a first linear behaviour following by a non linear behaviour. The results obtained in this study leads to a shear stress level higher than the results obtained in [53, 43] for an equivalent strain rate. The shear stress–strain curve obtained during this campaign were also compared to stress–strain curves of hight density poly-ethylen (HDPE) polymer obtained by Zhang and Moore [55] for two different strain rates (10^{-4} and 10^{-3} s^{-1}) in the Figure 9. One may noticed that mechanical behaviour of tested laminate seems similar to the mechanical behaviour of HDPE polymer. Therefore, as highlighted in the literature the mechanical behaviour of Tensylon® [±45°] seems strongly dependent on the mechanical behaviour of its matrix, *i.e.* HDPE. Moreover, strain rate seems to have an influence on the shear mechanical behaviour, and particularly on the elastic limit.

In the literature, different authors [14, 53] studied non linear behaviour of UHMWPE [±45°] Dyneema® laminate, in their case. They performed loading/unloading tests for one quasi-static strain rate [53] or for three strain rates. These authors shown a strong non linear behaviour [14, 53] which can be due to matrix damage, viscoplastic effects or friction between broken surfaces [53]. As previously said mechanical behaviour of [±45°] UHMWPE laminate is strongly dependent of matrix behaviour [53]. To the authors knowledge, there is no study of influence of strain rate on non linear behaviour of [±45°] Tensylon® laminate. The same experimental protocol than for [0°/90°] laminates were applied on [±45°] laminates (Figure 10). Three tests were performed for each configuration.

A first analysis of the influence of strain rate on the mechanical behaviour of Tensylon® [±45°] is performed from Figure 11. Shear stress–shear strain

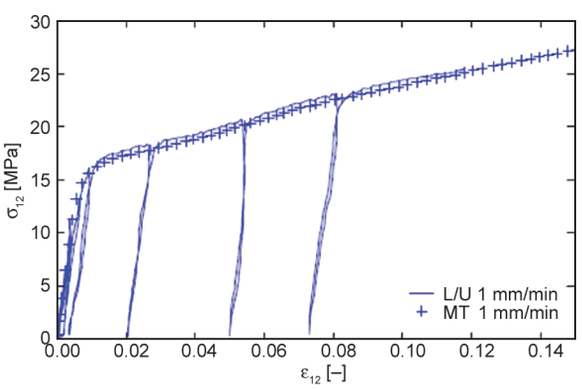

Figure 10. Comparison between stress–strain curves of the monotonous uniaxial tensile test and the loading/unloading uniaxial test performed at 1 mm/min on the Tensylon® $[\pm 45°]_{20}$.

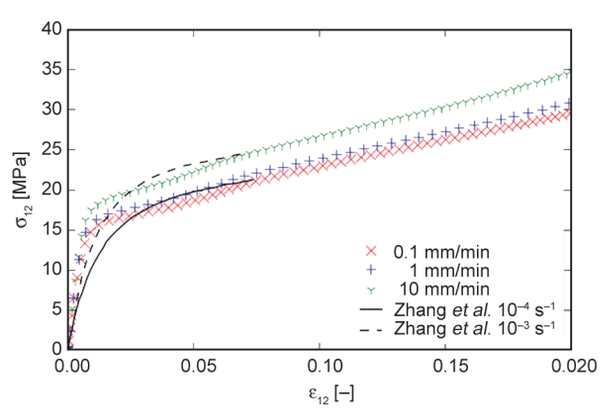

Figure 9. Tensylon® $[\pm 45°]_{20}$ shear stress–shear strain curves for uni-axial monotonous tensile tests at three different strain rates and at room temperature.

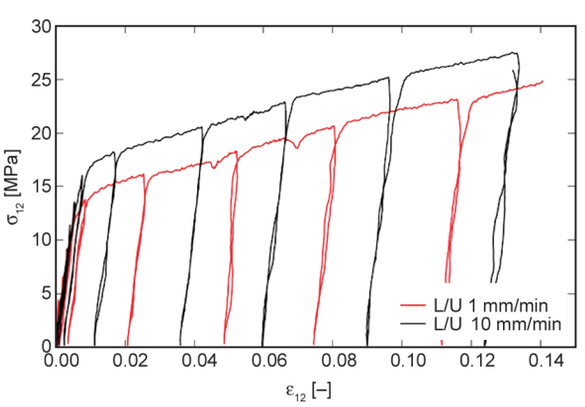

Figure 11. Tensylon® $[\pm 45°]_{20}$ stress–stravin curves for uniaxial loading/unloading tests at two different strain rates and at room temperature.

curve for loading/unloading tests performed at 0.1 and 10 mm/min point out tha strain rate influences the mechanical behaviour of studied material. Indeed, the maximum stress measured at 10 mm/min is 12% higher than the one measured at 0.1 mm/min.

3. Dynamic tests with split Hopkinson tensile bars system

In this study, a SHTB setup was used, based on the principle of split Hopkinson bar theory [37].

Figure 12 shows an illustration of such a setup. It consists of an incident bar and a transmitted one. A tubular striker slides on the incident bar and impacts its stepped end used as anvil. A compressive wave is then generated. When reaching the end of the anvil, this wave is reflected as a tensile wave that propagates along the incident bar. Note that a shock absorber can be used to limit the displacement resulting from the impact. Finally, strain gauges are positioned on both bars.

The stress and the strain in the specimen can be recovered using the strain gauges signals and the SHTB analysis [37, 38]. This operation however requires to ensure that the system is at equilibrium, *i.e.* both of its ends are simultaneously loaded with the same force. We denote by ε_I the incident strain, ε_R the strain due to the reflected wave in the incident bar and ε_T the strain in the transmitted bar (Figure 13).

The specimen is considered to be at equilibrium if strains at both ends of the sample are equal during the test (Equation (1)):

$$\varepsilon_I + \varepsilon_R = \varepsilon_T \tag{1}$$

Provided Equation (1) is satisfied, the strain and the strain rate in the specimen are respectively (Equation (2)):

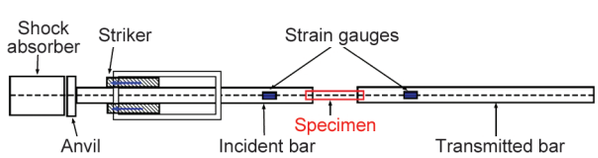

Figure 12. Split Hopkinson tensile bar experimental setup.

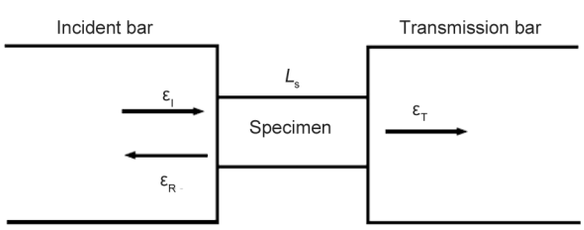

Figure 13. Definition of the quantities evaluated during a test.

$$\varepsilon_{sp} = -2\frac{C_b}{L_s}\int_0^t \varepsilon_R \, dt \quad \text{and} \quad \dot{\varepsilon}_{sp} = -2\frac{C_b}{L_s}\varepsilon_R \tag{2}$$

where C_b the wave velocity in the bar, and L_s the initial length of the specimen.

Under the same assumption and based on one wave analysis, the engineering stress σ_{sp} in the specimen can written as (Equation (3)):

$$\sigma_{sp} = \frac{A_b}{A_{sp0}} E_b \varepsilon_T \tag{3}$$

where A_b and A_{sp0} are respectively the bar and the specimen cross-section areas. E_b is the Young modulus of the bars.

The sptlit Hopkinson tensile test system at ENSTA Bretagne, Brest, France, was developed by Tema Concept, at Chanteloup-les-Vignes, France, in the 1990s. The bars are made of Maraging C350, produced by Smithmetal, Biggleswade, UK. One can note that the impedance mismatch between the bars and the sample is significant however the ambition of this study is to reach the highest strain-rate with the existing bars, to get closer than that of actual strain rates encountered during ballistic impacts. Thus, no pulse shaper was used. In addition, Tensylon exhibited exceptional strength that the clamping system broke several times during preliminary tests, telling that an even softer material for respectively incident and transmitted bar would have broken the threats of the screwed clamps. The system configuration is summarised in Table 1. All the experiments presented in this work are performed at a temperature of 19 °C.

The strain of the incident and transmitted bars was measured with strain gauges K-CLY4-1-350 provided by HBM, Darmstadt, Germany, in full bridge configuration. All the signals were recorded using a Genesis HBM® acquisition system (Darmstadt, Germany) with an acquisition frequency of 2 MHz.

The strain gage voltage is converted into strain using Equation (4), and thus, the incident ε_I, reflected ε_R, and transmitted ε_T strains are obtained:

$$\varepsilon = \frac{2\Delta E_m}{k(1+\nu)\left(V - 2\frac{1-\nu}{1+\nu}\Delta E_m\right)} \tag{4}$$

Table 1. Properties of the split Hopkinson tensile bars used.

D [mm]	Striker length [mm]	E_b [GPa]	C_b [m/s]	Pressure [bar]	$V_{striker}$ [m/s]
22	400	183.7	4847	1 to 7	5 to 26

where ε, ΔE_m, k, ν and V are respectively the strain, the bridge output voltage, the gage factor, Poisson ratio and the bridge supply voltage.

Previous studies reported a possible underestimation of ε_{sp} due to edge effects [37, 48]. Consequently, Digital Image Correlation (DIC) was used as a second method to measure the strain in the specimen in order to deny or validate this assumption. For that purpose, a Photron® SAX-2 high-speed camera, commercialized by Photron, Tokyo, Japan, was used with two spotlights, as shown in Figure 14. The frame rate was set to 200 000 frames/s. The image analysis was performed with the GOM correlate® software (GOM, Gmbh, Heverlee, Germany) [41].

In the following, the two mounting systems that were used in the experiments are presented. The design of the first mounting system was inspired by previous works [34]. The corresponding drawings are shown in Figure 15. The clamps were screwed directly in the incident and transmitted bars. They are composed of a preform with a slot nut, which allows to clamp the specimen. The specimen drawing is introduced in Figure 15 on the right. The thickness of the specimen is 2.40 mm. The length of the useful zone of the specimen is 16 mm.

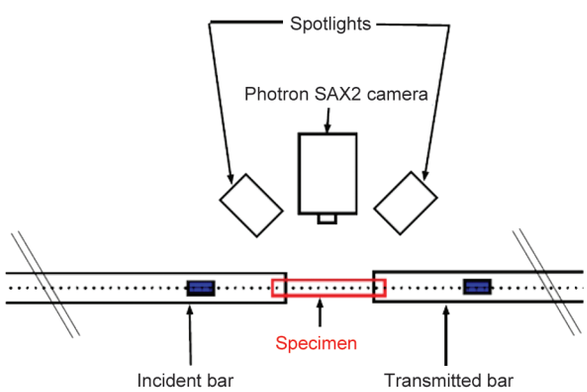

Figure 14. Sketch of the Digital Image Correlation (DIC) apparatus.

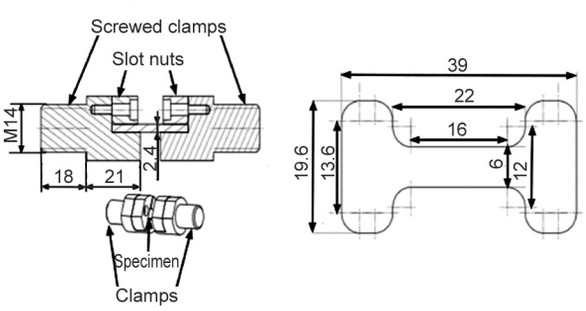

Figure 15. First mounting system proposed (left) and of the corresponding specimen (right). Dimensions are in mm.

With this mounting system, three loading pressures were tested: 2, 2.5 and 2.75 bar in order to cover a sufficiently large range of strain rates. The $[0°/90°]_{20}$ and $[\pm 45°]_{20}$ laminates were tested. With such a configuration, three major issues were reported, shown in Figure 16. First, for loading pressures greater than 2.75 bar, the slot nut loosened and the clamps opened. This phenomenon would even occur at 2.75 bar. As a consequence, the specimen was not bound correctly any more (Figure 16). Moreover, an important shear inside the clamp was observed during the test (Figure 16 bottom). Finally, the amplitude of the transmitted signal was very low, around 0.1 mV, and perturbations were observed in the reflected signal, probably due to the poor resulting binding conditions. This first mounting system was therefore considered not appropriate to study the mechanical behaviour of UHMWPE composite materials.

In order to reduce the influence of the aforementioned problems, a second mounting system was designed. The corresponding drawing plans are shown in Figure 17. This system is composed of a preform

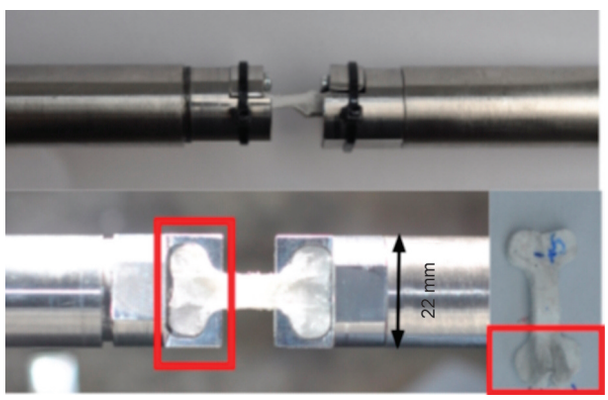

Figure 16. Mounting system, shown in Figure 4, after an experiment performed on Tensylon® $[0°/90°]_{20}$. The loading pressure was 2.75 bar. Top: image taken directly after the experiment, bottom left: setup conditions after opening the clamps, bottom right: photograph of the specimen after impact.

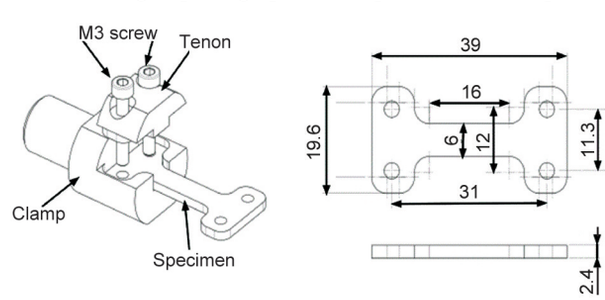

Figure 17. Description of the second mounting system (on the left) and of the corresponding specimen (on the right). Dimensions are in mm.

with a tenon which allows a better binding than in the previous mounting system. Moreover, two screws by clamps were added. These screws allow to perform a stop by obstacle as Russell *et al*. [14] and Levi-Sasson *et al*. [19] used when performing quasi-static tests on a DYNEEMA®, DSM, Herleen, The Netherlands, another UHMWPE composite material.

During the preliminary campaign, no holding and clamping problems were observed. No limitation was highlighted. The tests were performed on the two laminates and for three pressure loadings up to 6 bar. Nevertheless, another difficulty arose: for pressure higher than 3 bar, the painted speckle did not hold. Consequently, another type of speckle with pencil ink was used.

Finally, split Hopkinson tensile tests were performed for the two stacking sequences $[0°/90°]_{20}$ and $[\pm45°]_{20}$ for three different pressures: 4, 5 and 6 bar. For each configuration five tests were performed.

3.1. Dynamic tests on the $[\pm45°]_{20}$ laminate

In this section, the results obtained for the Tensylon® $[\pm45°]_{20}$ for three loading pressures are presented. Figure 18 shows the strain as a function of time for SHTB analysis and DIC measurements. The SHTB strain analysis, εsp and the DIC one, ε_{xx}^{DIC}, exhibit the same behaviour.

The DIC method therefore appears to be reliable to measure the strain as mentioned in [37, 40]. In order to get rid of the experimental noise, it has been proposed to model time evolution of $\dot{\varepsilon}^{DIC}$ with a bi-linear model, represented in grey solid line in Figure 18. The bilinear aspect is interpreted by an elastic phase until fibers turn to disconnect to one another. The specimen is then delaminated and is expanding even with a low stress increment, like an accordion. This

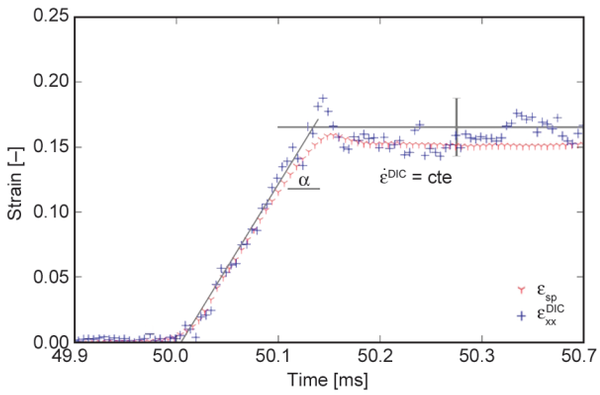

Figure 18. Time evolution of the strain in the specimen for a SHTB test performed at 6 bar on Tensylon® $[\pm45°]_{20}$.
+ – DIC measurements, Y – strain gauge results. The grey, solid line is a bi-linear model, the plateau being centered on the average value.

expansion was reported in dynamic condition by Lässig *et al*. [42].

The evolution of the strain rate as a function of time is now investigated. The strain rate values were obtained by numerical derivation of ε_{sp} and ε_{xx}^{DIC}. Figure 19 shows the corresponding results for three loading pressures for DIC results on the left side and for SHTB analysis on the right side.

Whatever the loading pressure and the strain measurement method used, the strain rate always exhibits the same pattern: a first, rapid increase (≈1000 s^{-1} in less than 0.05 ms), a plateau for ≈0.07 ms that is actually disturb by transient effects or speckle crackling, and a rapid decrease (≈1000 s^{-1} in ≈0.05 ms).

The strain rate $\dot{\varepsilon}_{sp}$ and $\dot{\varepsilon}_{xx}^{DIC}$ are respectively computed by taking the average value in what should theoretically be a plateau region at least at the beginning of the plateau and the slope α of the signal model

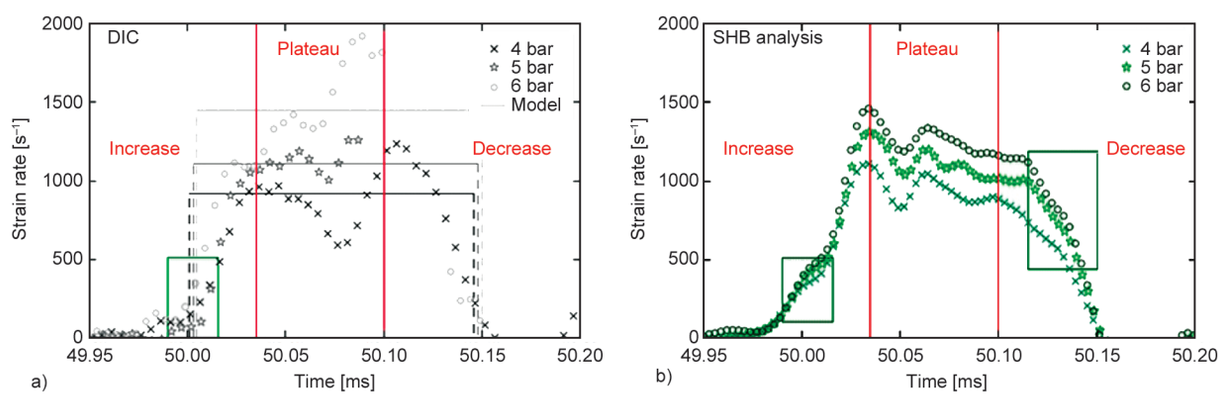

Figure 19. Evolution of the strain rate with the time for SHTB tests performed at three different loading pressures on the Tensylon® $[\pm45°]_{20}$. Both results from DIC (a) and strain gauges (b) are shown.

Table 2. Strain rates values obtained with SHTB analysis and DIC method.

Load pressures	$V_{striker}$ [m/s]	$\dot{\varepsilon}_{sp}$	$\dot{\varepsilon}_{xx}^{DIC}$	$\frac{\lvert\dot{\varepsilon}_{sp}-\dot{\varepsilon}_{xx}^{DIC}\rvert}{\dot{\varepsilon}_{sp}}$
4 bar	15	946 s^{-1} ±1%	915 s^{-1} ±1%	3%
5 bar	18	1131 s^{-1} ±1%	1110 s^{-1} ±1%	2%
6 bar	21	1275 s^{-1} ±1%	1450 s^{-1} ±1%	12%

evaluation as shown in Figure 7. The strain rates values are summarised in Table 2.

Whatever the strain measurement method, a perturbation in the first increase of the strain rate is observed at t = 50 ms. A second perturbation in the first decrease is visible at 50.12 ms on the $\dot{\varepsilon}_{sp}$ curve. A loss of information on the $\dot{\varepsilon}_{xx}^{DIC}$ signal on this time range prevents from any conclusion for this method.

To understand the origin of those two perturbations, strains corresponding to incident and reflected stress waves, ε_I and ε_R, were plotted on a same graph (Figure 20) for a test performed at 6 bar. The strain ε_R associated with the reflected stress wave was temporally shifted, considering the wave velocity and the gauge position. The same perturbations are always observed on the reflected signal and at the same time. These features could be due to an out-of-equilibrium state at this time of the test or to a perturbation generated by the bar geometry. As stated in previous studies [37, 40], results obtained with a direct method, *i.e*, DIC, are to be preferred. Thanks to DIC results, the shear strain is evaluated by Equation (5):

$$\varepsilon_{12} = \frac{\left|\varepsilon_{xx}^{DIC} - \varepsilon_{yy}^{DIC}\right|}{2} \tag{5}$$

For example, the different strain quantities obtained for a test performed at 6 bar are plotted in Figure 21. As for Figure 20, a perturbation can be observed on

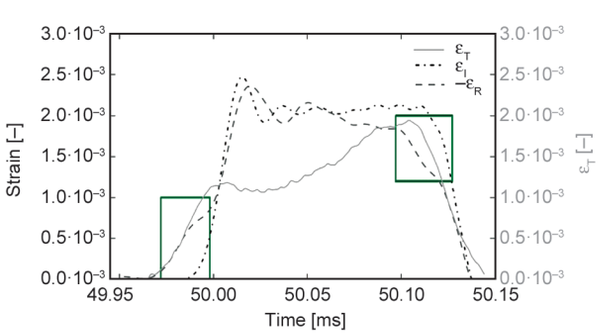

Figure 20. Incident (dashed dotted line), reflected (dotted line) and transmitted (solid line) strains as a function of time for SHTB tests at 6 bar on Tensylon® $[\pm45°]_{20}$.

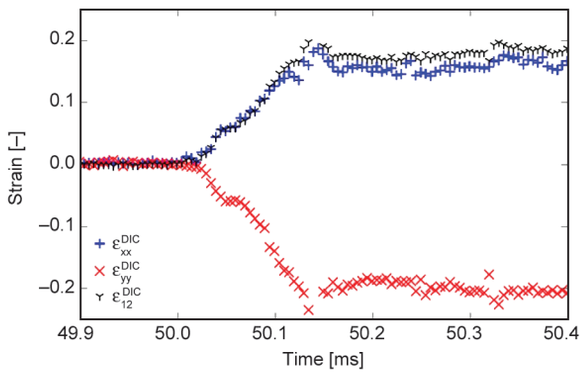

Figure 21. Time evolution of the strain obtained by DIC (ε_{xx}, ε_{yy} and ε_{12}) in the specimen for a SHTB test performed at 6 bar on Tensylon® $[\pm45°]_{20}$.

the different strain signals round 50.12 ms. One may notice that the shear strain ε_{12} and the longitudinal strain ε_{xx}^{DIC} are equal at any time, as expected for a $[\pm45°]_{20}$ laminate. The shear stress reads (Equation (6)):

$$\sigma_{12} = \frac{A_b}{2A_{sp0}} E_b \varepsilon_T \tag{6}$$

The shear stress–strain curves obtained with SHTB tests are compared with those of quasi-static uniaxial tensile test performed on Tensylon® $[\pm45°]_{20}$ with an electro-mechanic jack INSTRON® 5969, (Norwood, USA) following the standard EN-ISO 14129 [43] except for the shape specimen which is taken from [14]. At low shear strains ($\varepsilon < 0.02$), the quasi-static and dynamic data points seem to exhibit the same behaviour (Figure 21). For strain above 0.02, the evolution of the shear stress with the shear strain is much slower in quasi-static regime. Moreover, in this regime, the strain rate seems to have a significant effect on the stress value (Figure 22). This was observed for all the tests. As an example, for a strain of 0.15, an increase of 45% in the stress is observed between the quasi-static ($\dot{\varepsilon} = 2 \cdot 10^{-5}$ s^{-1}) and the dynamic configuration ($\dot{\varepsilon}$ = 1450 s^{-1}). These results are partially in agreement with Russell *et al.* [14] since they highlighted an important influence of strain rate on the mechanical behaviour (linear and nonlinear) of Dyneema® [±45°] laminate, for tests performed until 10^{-2} s^{-1}. Other work has shown that the mechanical behaviour of [±45°] laminate is strongly dependent on the matrix behaviour [44–46]. For Dyneema®, the matrix is poly-urethan whereas for Tensylon®, the matrix is poly-ethylene. This increase in shear stress can be explained by the fact

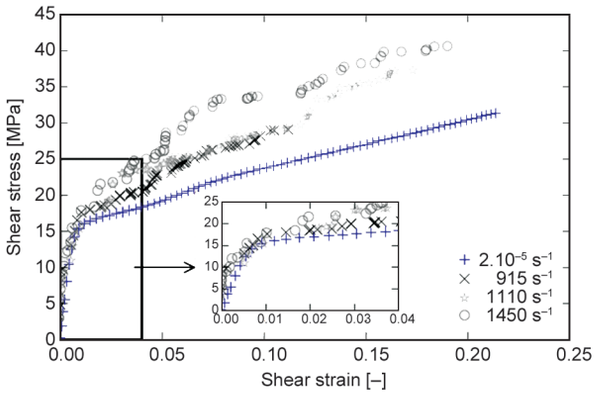

Figure 22. Shear stress - strain curves for split Hopkinson tensile tests and for uni-axial quasi-static tests performed on the Tensylon® $[\pm 45°]_{20}$ for four strain rates.

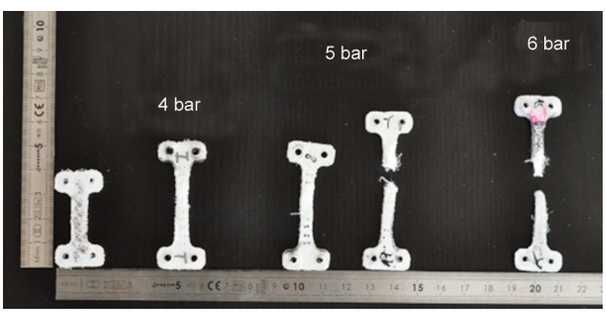

Figure 23. Post-mortem specimen of Tensylon® $[\pm 45°]_{20}$ at various pressures. The reference specimen before test is shown on the far left.

that fibres are on the way to the longitudinal direction and, thus, tend to work more in tension.

Finally, the post mortem specimens were analysed (Figure 23). For a loading pressure of 4 bar, none of the specimens failed. Conversely, failure was observed at higher pressures. At 5 bar, failure was observed in 60% of cases whereas specimens would systematically fail at 6 bar. Figure 21 also shows that the failure of the specimen always occurred in the useful zone, whatever the loading pressure. The proposed mounting system is therefore suitable for Tensylon® specimens with [±45°] orientation.

The mounting system was also used to perform tests on Tensylon® $[0°/90°]_{20}$ laminate. The obtained results on the $[0°/90°]_{20}$ have raised a number of issues introduced in the following section.

3.2. Dynamic tests on the $[0°/90°]_{20}$ laminate

All the results presented in this section were obtained by strain gauge signals of the incident and transmitted bars with the split Hopkinson bar analysis.

The influence of the loading pressure on the strain rate was first investigated. The evolution of the strain

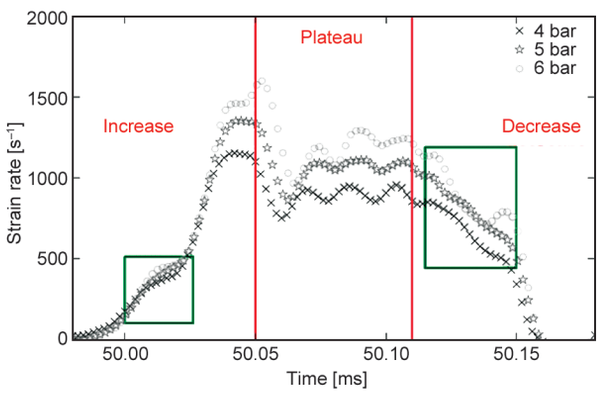

Figure 24. Evolution of the strain rate with time for split Hopkinson tensile tests performed on the Tensylon® $[0°/90°]_{20}$ for three different loading pressures.

rate with time was measured for three loading pressures: 4, 5 and 6 bar. The corresponding strain rate evolution with time is shown in Figure 24. Whatever the loading pressure, the strain rate always exhibits the same pattern: a first, rapid increase (≈1000 s^{-1} in less than 0.1 ms), a plateau for ≈0.05 ms, and a rapid decrease (≈1000 s^{-1} in ≈0.03 ms). The representative strain rate is computed by taking the average value in the flat region. Hence, for loading pressure of 4, 5 and 6 bar, the corresponding strain rate are 932, 1099 and 1300 s^{-1} respectively. Note that two perturbations are visible on the increase and decrease front (Figure 13). These phenomena were previously highlighted.

Figure 25 shows the stress–strain curves for the $[0°/90°]_{20}$ laminate for four different strain rates. The curves at 932, 1099 and 1300 s^{-1} were obtained with

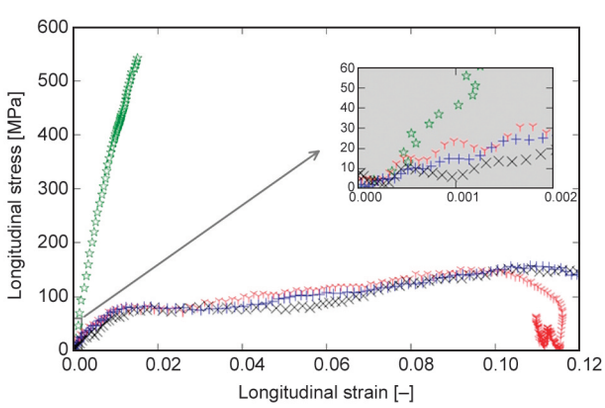

Figure 25. Comparison between the longitudinal stress–strain obtained for split Hopkinson tensile tests performed at three strain rates (Y – 932 s^{-1}, + – 1099 s^{-1} and × – 1300 s^{-1}) and longitudinal stress–strain obtained for uni-axial quasi-static tensile tests (at 10^{-3} s^{-1}(in green stars)) on the Tensylon® $[0°/90°]_{20}$.

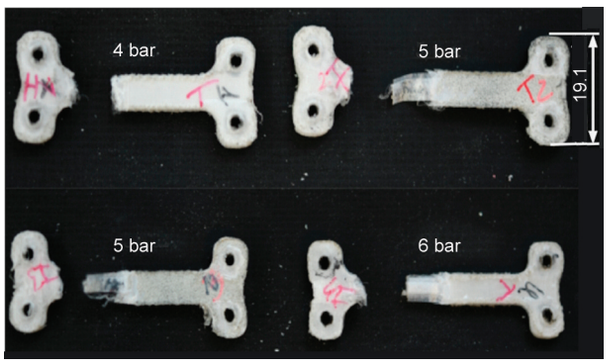

Figure 26. Post-mortem specimens of Tensylon® $[0°/90°]_{20}$ at various loading pressures. Dimensions are in mm.

the SHTB setup while that at 10^{-3} s^{-1} corresponds to a quasi-static test performed on an electro-mechanic jack INSTRON® 5969 following the standard EN-ISO 527 [47] except for the shape specimen shape which is taken from [14]. For stress under 30 MPa both quasi-static and dynamic curves show the same trend (Figure 25). Above this threshold, the quasi-static curve exhibits a linear trend until failure at around 550 MPa while the dynamic curves saturate quickly, reaching a maximum stress of ≈110 MPa whatever the strain rate. This behaviour differs from the quasi-static one and is not in agreement with observations reported in the literature [28]. To characterise this phenomenon, a post-mortem analysis was performed on the specimen.

Photographs of four different post-mortem specimens are presented in Figure 26. Two specimens were tested at 5 bar and the two others at 4 and 6 bar. The failure of the specimen does not occur in the useful zone of the specimen but is always at the level of the incident clamp (Figure 26). This indicates a stress concentration at the section change near the incident clamp. The test is therefore not reliable and a new concept will be designed in order to relocate the failure in the middle of the $[0°/90°]_{20}$ specimen.

4. Conclusions

A major issue of the proposed works was to study the influence of strain rate on the mechanical behaviour of UHMWPE, and particularly of two laminates [0°/90°] and [±45°] of Tensylon®. In order to answer to this issue, two different experimental campaign have been performed static and dynamic test.

During the first experimental campaign, uniaxial monotonous and loading/unloading uniaxial tensile tests have been performed on the two laminates and for three different displacement velocity. First of all, the mechanical behaviour of the two laminates can be decomposed into two parts: a first linear part following by a nonlinear behaviour. The influence of strain rate on the elastic properties of these two laminates could be evaluated with the monotonous loading. For the range of strain rate studied, *i.e.* $\dot{\varepsilon} = [\cdot 10^{-5}; 1 \cdot 10^{-3}$ s^{-1}, when the strain rate increased the Young modulus, the shear modulus and the corresponding elastic limit also increased. The nonlinear behaviour of two laminates is evaluated with loading/unloading uniaxial tensile tests. For the [0°/90°] laminates, the irreversible strain appears from the first cycles and is strain rate dependent. When the strain rate increased the irreversible strain measured decreased. For the $[\pm 45°]_{20}$ laminate. The irreversible strain is negligible until the maximum shear stress applied exceeds the elastic limit. According to the observations done during this campaign, the various phenomena involved in the nonlinear behaviour of the two laminates seem to be different. The mechanical behaviour of [±45°] laminates is strongly dependent on the matrix mechanical behaviour in contrast with the mechanical behaviour of [0°/90°] laminates, which seems to be closer than the fibre mechanical behaviour.

During the second campaign, the mechanical behaviour of Tensylon in the intermediate strain rate regime (from 900 to 1500 s^{-1}) was investigated. To this end, split Hopkinson bar testing campaign on Tensylon® for two stacking sequences of respectively $[0°/90°]_{20}$ and $[\pm 45°]_{20}$, and three loading pressures were investigated. A mounting system was especially designed for overcoming clamps loosening and specimen ripping in the grips. It was successfully implemented as a direct method to measure the strain by Digital Image Correlation. The mounting system and specimen shape were indicated for the $[\pm 45°]_{20}$ laminate. Such a setup could, therefore, be used for various composite materials. However, the setup did not appear to be suitable for a $[0°/90°]_{20}$ laminate as stress concentration was reported near the clamps. Another clamp design is currently being developed.

Regarding the $[\pm 45°]_{20}$ laminate, the strain gauge measurements were compared to those from DIC ones were compared. A significant difference on the strain and strain rate levels was observed. The presence of various perturbations on the strain gauge signal led to only consider the DIC results to characterise the mechanical behaviour of UHMWPE for

the explored strain rate range (900 to 1500 s^{-1}). Experimental trends were compared to those obtained in a quasi-static configuration. For low strains, the mechanical response appears to be universal. Conversely, a significant effect of the strain rate on the stress level was observed for higher strain rates.

A logical prospect to this works would be to carry out additional tests by the use of a pulse shaper to access strain rates in between 100 to 900 s^{-1} in order to consolidate the strain-rate dependency. That experimental part could be completed by numerical simulations, allowing to perform a full parametric study and confirm or disprove the different assumptions upon which this study is based. The validation of the experimental setup on various composite materials and the design of a new mounting system for the $[0°/90°]_{20}$ laminate are beyond the scope of the present work and will be the topic of future investigations.

Acknowledgements

The authors would like to thank the Agence Innovation Défense of the DGA (Direction Générale de l'Armement, the French Armament procurement Directorate) for funding the DYNACOMPPE research project and equipment that contributed to this work, the IUT Brest – Morlaix (Institut Universitaire Technologique) and particularly T. Bonnemains and E. Lolive for their assistance for the specimens cutting by waterjet. The authors also would like to thank TenCate Advanced Armour for providing the Tensylon®, especially Pauline Respaud and Jean Beugels.

References

[1] Domun N., Kaboglu C., Paton K. R., Dear J. P., Liu J., Blackman B. R., Liaghat G., Hadavinia H.: Ballistic impact behaviour of glass fibre reinforced polymer composite with 1D/2D nanomodified epoxy matrices. Composites Part B: Engineering, **167**, 497–506 (2019). https://doi.org/10.1016/j.compositesb.2019.03.024

[2] Gellert E., Cimpoeru S., Woodward R.: A study of the effect of target thickness on the ballistic perforation of glass-fibre-reinforced plastic composites. International Journal of Impact Engineering, **24**, 445–456 (2000). https://doi.org/10.1016/S0734-743X(99)00175-X

[3] Onyechi P., Edelugo S., Chukwumuanya E., Obuka S.: Ballistic penetration response of glass fibre reinforced polyester (GFRP) composites: Body amour. International Journal of Scientific and Technology Research, **3**, 226–237 (2014).

[4] Cunniff P. M.: Decoupled response of textile body armor. in 'Proceedings of the 18th International Symposium of Ballistics, Boca Raton, USA' 814–821 (1999).

[5] Alil L-C., Arrigoni M., Badea S., Ginghină R., Matache L-C., Mostovykh P.: Ballistic study of Tensylon®-based panels. Express Polymer Letters, **12**, 491–504 (2018). https://doi.org/10.3144/expresspolymlett.2018.42

[6] Greenhalgh E. S., Bloodworth V. M., Iannucci L., Pope D.: Fractographic observations on Dyneema® composites under ballistic impact. Composites Part A: Applied Science and Manufacturing, **44**, 51–62 (2013). https://doi.org/10.1016/j.compositesa.2012.08.012

[7] May M., Nossek M., Petrinic N., Hiermaier S., Thoma K.: Adaptive multi-scale modeling of high velocity impact on composite panels. Composites Part A: Applied Science and Manufacturing, **58**, 56–64 (2014). https://doi.org/10.1016/j.compositesa.2013.11.015

[8] Lidén E., Berlin R., Janzon B., Schantz B., Seeman T.: Some observations relating to behind-body armour blunt trauma effects caused by ballistic impact. The Journal of Trauma and Acute Care Surgery, **28**, 145–148 (1988). https://doi.org/10.1097/00005373-198801001-00029

[9] Gregori D., Scazzosi R., Nunes S. G., Amico S. C., Giglio M., Manes A.: Analytical and numerical modelling of high-velocity impact on multilayer alumina/aramid fiber composite ballistic shields: Improvement in modelling approaches. Composites Part B: Engineering, **187**, 107830 (2020). https://doi.org/10.1016/j.compositesb.2020.107830

[10] Lässig T., Nguyen L., May M., Riedel W., Heisserer U., van der Werff H., Hiermaier S.: A non-linear orthotropic hydrocode model for ultra-high molecular weight polyethylene in impact simulations. International Journal of Impact Engineering, **75**, 110–122 (2015). https://doi.org/10.1016/j.ijimpeng.2014.07.004

[11] Clegg R. A., White D. M., Riedel W., Harwick W.: Hypervelocity impact damage prediction in composites: Part I – Material model and characterisation. International Journal of Impact Engineering, **33**, 190–200 (2006). https://doi.org/10.1016/j.ijimpeng.2006.09.055

[12] Riedel W., Nahme H., White D. M., Clegg R. A.: Hypervelocity impact damage prediction in composites: Part II – Experimental investigations and simulations. International Journal of Impact Engineering, **33**, 670–680 (2006). https://doi.org/10.1016/j.ijimpeng.2006.09.052

[13] Wicklein M., Ryan S., White D. M., Clegg R. A.: Hypervelocity impact on CFRP: Testing, material modelling, and numerical simulation. International Journal of Impact Engineering, **35**, 1861–1869 (2008). https://doi.org/10.1016/j.ijimpeng.2008.07.015

[14] Russell B. P., Karthikeyan K., Deshpande V. S., Fleck N. A.: The high strain rate response of ultra high molecular-weight polyethylene: From fibre to laminate. International Journal of Impact Engineering, **60**, 1–9 (2013). https://doi.org/10.1016/j.ijimpeng.2013.03.010

[15] Bensaada R., El Malki Alaoui A., Darut G., Costil S., Arrigoni M.: Towards hybridization of ultra-high molecular weight polyethylene composites by thermally sprayed alumina: Feasibility and bond strength assessment. Materials and Design, **227**, 111779 (2023). https://doi.org/10.1016/j.matdes.2023.111779

[16] Alil L. C., Arrigoni M., Badea S., M., Barbu C., Istrate M., Mostovykh P. S.: On the constitutive law for the mechanical quasi-static response of criss-cross composites (on the example of UHMWPE). Human Factors and Mechanical Engineering for Defense and Safety, **1**, 4 (2017). https://doi.org/10.1007/s41314-017-0006-5

[17] Dessain B., Moulaert O., Keunings R., Bunsell A. R.: Solid phase change controlling the tensile and creep behaviour of gel-spun high-modulus polyethylene fibres. Journal of Materials Science, **27**, 4515–4522 (1992). https://doi.org/10.1007/BF00541588

[18] Iannucci L., Pope D.: High velocity impact and armour design. Express Polymer Letters, **5**, 262–272 (2011). https://doi.org/10.3144/expresspolymlett.2011.26

[19] Levi-Sasson A., Meshi I., Mustacchi S., Amarilio I., Benes D., Favorsky V., Eliasy R., Aboudi J., Haj-Ali R.: Experimental determination of linear and nonlinear mechanical properties of laminated soft composite material system. Composites Part B: Engineering, **57**, 96–104 (2014). https://doi.org/10.1016/j.compositesb.2013.09.043

[20] Roiron C., Lainé E., Grandidier J-C., Olivier D., Garois N., Vix C.: Study of the thermomechanical behavior of UHMWPE yarns under different loading paths. Polymer Testing, **89**, 106717 (2020). https://doi.org/10.1016/j.polymertesting.2020.106717

[21] Matache L-C., Alil L-C., Rotariu T., Sandu S., Puica C., Barbu C., Zecheru T.: Numerical validation of a constitutive model for uhmwpe-based composites at high strain rates. University Politehnica of Bucharest Scientific Bulletin Series B: Chemistry and Materials Sciences, **80**, 229–246 (2018).

[22] Alil L. C., Matache L. C., Sandu S. M.: Numerical simulation of a ballistic impact on Tensylon® UHMWPE laminates using the plastic kinematic model in LS-Dyna®. Journal of Military Technology, **1**, 43–50 (2018). https://doi.org/10.32754/JMT.2018.1.08

[23] Freitas C. J., Bigger R. P., Scott N., LaSala V., MacKiewicz J.: Composite materials dynamic back face deflection characteristics during ballistic impact. Journal of Composite Materials, **48**, 1475–1486 (2014). https://doi.org/10.1177/0021998313487934

[24] Luminita C., Arrigoni M., Deleanu L., Istrate M.: Assessment of delamination in Tensylon® UHMWPE composites by laser-induced shock. Materiale Plastice, **55**, 364–371 (2018).

[25] Nguyen L. H., Lässig T. R., Ryan S., Riedel W., Mouritz A. P., Orifici A. C.: A methodology for hydrocode analysis of ultra-high molecular weight polyethylene composite under ballistic impact. Composites Part A: Applied Science and Manufacturing, **84**, 224–235 (2016). https://doi.org/10.1016/j.compositesa.2016.01.014

[26] Rodolfo R., Tlalpa Galan M. A., Carrillo J., Gamboa R.: Evaluation of ultra high molecular weight polyethylene (UHMWPE) anisotropic TM TM configuration sample of Tensylon, Dupont at medium velocity impact test. Mexican Journal of Materials Science and Engineering, **1**, 24–32 (2018).

[27] Zhang T. G., Satapathy S. S., Vargas-Gonzalez L. R., Walsh S.: Ballistic impact response of ultra-high-molecular-weight polyethylene (UHMWPE). Composite Structures, **133**, 191–201 (2015). https://doi.org/10.1016/j.compstruct.2015.06.081

[28] Li C., Guo H., He T., Tian X.: A rate-dependent constitutive model of piezoelectric thermoelasticity and structural thermo-electromechanical responses analysis to multilayered laminated piezoelectric smart composites. Applied Mathematical Modelling, **112**, 18–46 (2022). https://doi.org/10.1016/j.apm.2022.07.025

[29] Li C., Tian X., He T.: New insights on piezoelectric thermoelastic coupling and transient thermo-electromechanical responses of multi-layered piezoelectric laminated composite structure. European Journal of Mechanics-A/Solids, **91**, 104416 (2022). https://doi.org/10.1016/j.euromechsol.2021.104416

[30] Poulet T., Bracq A., Demarty Y., Lauro F., Bahlouli N.: Strain rate sensitivity of the in-plane mechanical properties of two UHMWPE thin ply composites. Polymer Testing, **127**, 108187 (2023). https://doi.org/10.1016/j.polymertesting.2023.108187

[31] Koh A., Shim V., Tan V.: Dynamic behaviour of UHMWPE yarns and addressing impedance mismatch effects of specimen clamps. International Journal of Impact Engineering, **37**, 324–332 (2010). https://doi.org/10.1016/j.ijimpeng.2009.10.008

[32] Hopkinson B. X.: A method of measuring the pressure produced in the detonation of high, explosives or by the impact of bullets. Philosophical Transactions of the Royal Society of London. Series A, Containing Papers of a Mathematical or Physical Character, **213**, 437–456 (1914). https://doi.org/10.1098/rsta.1914.0010

[33] Kolsky H.: An investigation of the mechanical properties of materials at very high rates of loading. Proceedings of the physical society. Section B, **62**, 676 (1949). https://doi.org/10.1088/0370-1301/62/11/302

[34] Ledford N., Paul H., Ganzenmüller G., May M., Höfemann M., Otto M., Petrinic N.: Investigations on specimen design and mounting for split Hopkinson tension bar (SHTB) experiments. EPJ Web of Conferences, **94**, 01049 (2015). https://doi.org/10.1051/epjconf/20159401049

[35] Verleysen P., Degrieck J., Verstraete T., van Slycken J.: Influence of specimen geometry on split Hopkinson tensile bar tests on sheet materials. Experimental Mechanics, **48**, 587 (2008). https://doi.org/10.1007/s11340-008-9149-x

[36] Verleysen P., Verhegghe B., Verstraete T., Degrieck J.: Numerical study of the influence of the specimen geometry on split Hopkinson bar tensile test results. Latin American Journal of Solids and Structures, **6**, 285–298 (2009).

[37] Chen W. W., Song B.: Split Hopkinson (Kolsky) bar: Design, testing and applications. Springer, New-York, (2011).

[38] Ninan L., Tsai J., Sun C. T.: Use of split Hopkinson pressure bar for testing off-axis composites. International Journal of Impact Engineering, **25**, 291–313 (2001). https://doi.org/10.1016/S0734-743X(00)00039-7

[39] Wang Y., Yin Z., Li H., Gao G., Zhang X.: Friction and wear characteristics of ultrahigh molecular weight polyethylene (UHMWPE) composites containing glass fibers and carbon fibers under dry and water-lubricated conditions. Wear, **380**, 42–51 (2017). https://doi.org/10.1016/j.wear.2017.03.006

[40] Gilat A., Schmidt T., Walker A.: Full field strain measurement in compression and tensile split Hopkinson bar experiments. Experimental Mechanics, **49**, 291–302 (2009). https://doi.org/10.1007/s11340-008-9157-x

[41] Casapu M., Fuiorea I., Arrigoni M.: Damage assessment through cyclic load-unload tensile tests for ply-level hybrid carbon fiber composites. Express Polymer Letters, **18**, 41–60 (2024). https://doi.org/10.3144/expresspolymlett.2024.4

[42] Lässig T., Bagusat F., Pfändler S., Gulde M., Heunoske D., Osterholz J., Stein W., Nahme H., May M.: Investigations on the spall and delamination behavior of UHMWPE composites. Composite Structures, **182**, 590–597 (2017). https://doi.org/10.1016/j.compstruct.2017.09.031

[43] NF EN ISO 14129: Fibre-reinforced plastic composites. Determination of the in-plane shear stress/shear strain response, including the in-plane shear modulus and strength, by the plus over minus 45 degrees tension test method (1998).

[44] Boumbimba R-M., Wang K., Bahlouli N., Ahzi S., Rémond Y., Addiego F.: Experimental investigation and micromechanical modeling of high strain rate compressive yield stress of a melt mixing polypropylene organoclay nanocomposites. Mechanics of Materials, **52**, 58–68 (2012). https://doi.org/10.1016/j.mechmat.2012.04.006

[45] Wang K., Ahzi S., Boumbimba R. M., Bahlouli N., Addiego F., Rémond Y.: Micromechanical modeling of the elastic behavior of polypropylene based organoclay nanocomposites under a wide range of temperatures and strain rates/frequencies. Mechanics of Materials, **64**, 56–68 (2013). https://doi.org/10.1016/j.mechmat.2013.04.009

[46] Raimondo L., Iannucci L., Robinson P., Curtis P.: Modelling of strain rate effects on matrix dominated elastic and failure properties of unidirectional fibre-reinforced polymer-matrix composites. Composites Science and Technology, **72**, 819–827 (2012). https://doi.org/10.1016/j.compscitech.2012.02.011

[47] NF EN ISO 527-4: Plastics – Determination of tensile properties – Part 4: Test conditions for isotropic and orthotropic fibre-reinforced plastic composites (1997).

[48] Berthe J., Brieu M., Deletombe E., Portemont G.: Temperature effects on the time dependent viscoelastic behaviour of carbon/epoxy composite materials: Application to T700GC/M21. Materials and Design, **62**, 241–246 (2014). https://doi.org/10.1016/j.matdes.2014.05.025

[49] Kromm F., Lorriot T., Coutand B., Harry R., Quenisset J.: Tensile and creep properties of ultra high molecular weight PE fibres. Polymer Testing, **22**, 463–470 (2003). https://doi.org/10.1016/S0142-9418(02)00127-7

[50] Castres M., Berthe J., Brieu M., Deletombe E.: A strain rate and temperature dependent criterion to describe the linear–non linear behaviour's transition of organic matrix composite materials in shear: Application to T700GC/M21. Mechanics of Materials, **124**, 100–105 (2018). https://doi.org/10.1016/j.mechmat.2018.06.002

[51] Castres M., Berthe J., Deletombe E., Brieu M.: Experimental evaluation of the elastic limit of carbon-fibre reinforced epoxy composites under a large range of strain rate and temperature conditions. Strain, **53**, e12248 (2017). https://doi.org/10.1111/str.12248

[52] Heisserer U., van der Werff H., Hendrix J.: Ballistic depth of penetration studies in dyneema composites. in '27th International Symposium on Ballistics, Freiburg, Germany' 1936–1943 (2013).

[53] Iannucci L., Pope D., Dalzell M.: A constitutive model for dyneema UD composites. in '17th International Conference on Composite Materials, Edinburgh, United Kingdom' 27–31 (2009).

[54] Vyas G., Pinho S., Robinson P.: Constitutive modelling of fibre-reinforced composites with unidirectional plies using a plasticity-based approach. Composites Science and Technology, **71**, 1068–1074 (2011). https://doi.org/10.1016/j.compscitech.2011.03.009

[55] Zhang C., Moore I. D.: Nonlinear mechanical response of high density polyethylene. Part I: Experimental investigation and model evaluation. Polymer Engineering and Science, **37**, 404–413 (1997). https://doi.org/10.1002/pen.11683